Published in final edited form as:
Dev Dyn. 2011 October ; 240(10): 2364–2377. doi:10.1002/dvdy.22730.

A High Resolution Molecular Atlas of the Fetal Mouse Lower Urogenital Tract

Lisa L. Abler[1], **Kimberly P. Keil**[1], **Vatsal Mehta**[1], **Pinak S. Joshi**[1], **Christopher T. Schmitz**[1], and **Chad M. Vezina**[1,*]

[1]University of Wisconsin, Department of Comparative Biosciences

Abstract

Epithelial-stromal interactions in the lower urogenital tract (LUT) are integral to prostatic and seminal vesicle development in males, vaginal and uterine development in females, and urethral development in both sexes. Gene expression profiling of isolated LUT stroma and epithelium has unraveled mechanisms of LUT development, but such studies are confounded by heterogeneous and ill-defined cell sub-populations contained within each tissue compartment. We used *in situ* hybridization to synthesize a high-resolution molecular atlas of 17 days post coitus fetal mouse LUT. We identified mRNAs that mark selective cell populations of the seminal vesicle, ejaculatory duct, prostate, urethra and vagina, subdividing these tissues into 16 stromal and 8 epithelial sub-compartments. These results provide a powerful tool for mapping LUT gene expression patterns and also reveal previously uncharacterized sub-compartments that may play mechanistic roles in LUT development of which we were previously unaware.

Keywords

Prostate; seminal vesicle; urethra; urogenital sinus; urothelium; vagina; development; vasculature; mouse

INTRODUCTION

A spectrum of birth defects arises from malformations of the lower urogenital tract (LUT), including but not limited to urorectal fistula, posterior urethral valves, ectopic ureter, ectopic mesonephric (Wolffian) duct, ectopic or persistent paramesonephric (MÜllerian) duct, and malformations or agenesis of prostate and seminal vesicle. An improved understanding of normal LUT development would shed light on how these birth defects occur. It would also reveal new growth mechanisms that may be inappropriately reawakened in adult LUT diseases such as benign prostatic hyperplasia.

Epithelial-mesenchymal signaling is required for morphogenesis of most LUT tissues, including uterus and vagina (Price et al., 1977; Kurita et al., 2001), prostate (Cunha and Lung, 1978; Lasnitzki and Mizuno, 1980) and seminal vesicle (Wilson et al., 1981; Higgins et al., 1989; Tomaszewski et al., 2007). Stroma isolated from fetal prostate and seminal vesicle instructs *de novo* morphogenesis of these tissues from endoderm cells not normally programmed to form them (Cunha et al., 1983; Higgins et al., 1989), indicating that stromal cell populations orchestrate at least some aspects of LUT morphogenesis. Yet, the hormonally-induced stromal signaling pathway(s) required for morphogenesis of prostate,

[*]**Correspondence:** University of Wisconsin-Madison Dept. Comparative Biosciences School of Veterinary Medicine 1656 Linden Drive Madison, WI 53706 Phone (608) 890-3235 Fax (608) 262-7420 cmvezina@wisc.edu.

seminal vesicle, and other LUT tissues remains poorly understood. The LUT stromal cell sub-populations that produce morphogenetic stimuli are largely unknown and there is little insight about whether all or only a subset of LUT epithelial cells responds to these stimuli.

Mechanistic studies of late-stage LUT development are challenging due to the anatomical complexity of this region. Six epithelial tubes (two ureters, two MÜllerian ducts, and two Wolffian ducts) converge in close proximity to drain into the bladder and definitive urogenital sinus (UGS) portion of the pelvic urethra. Pelvic ganglia and two major fetal arteries (umbilical arteries) flank the lateral UGS aspects. In male fetuses, prostate, seminal vesicle and urethral glands arise from or nearby the UGS during approximately the same gestational period. At about the same time in female fetuses, MÜllerian duct-derived epithelium differentiates into vagina. The fact that tissue compartment boundaries are poorly defined and often overlap presents a formidable challenge to investigators who wish to study developmental mechanisms of one LUT tissue in isolation from others.

For reasons outlined above, there is a need to improve the resolution of developing mouse LUT anatomy. It is also crucial to identify specific cell and tissue markers that distinguish LUT tissue constituents and subdivide epithelium and stroma into specific layers and sub-compartments in order to generate new markers and tools for continuing LUT research. The goal of this study was to identify mRNAs that selectively mark fetal male and female mouse LUT tissue sub-compartments in collaboration with the GenitoUrinary Development Molecular Anatomy Project (GUDMAP), a consortium of laboratories dedicated to facilitating genitourinary tract research. We focused on 17 dpc mouse LUT anatomy, an embryonic stage when prostate and seminal vesicle glandular morphogenesis begins in males. *In situ* hybridization (ISH) was used to screen expression patterns of 71 different genes in 17 dpc male and female LUT and identify selective markers of LUT stromal and epithelial cell sub-populations. We identified selective markers for urothelium, smooth muscle, vasculature, prostatic buds, mesenchymal and epithelial components of Wolffian and MÜllerian ducts, and presumptive neural crest-derived cells, macrophages and interstitial cells of Cajal (ICC).

Recently, members of the GUDMAP consortium completed a high resolution molecular atlas of the developing mouse kidney (Brunskill et al., 2008). Like the LUT, the kidney is anatomically complex. Selective mRNA markers of the various kidney compartments, once identified, were used to purify renal cell sub-populations in order to conduct global gene expression profiling and reveal more specific cell markers that can be used for transgenic mouse synthesis, and cell fate mapping (Thiagarajan et al., 2011). Our study emulates the kidney molecular atlas project. Our results resolve a high-resolution LUT anatomy that will serve as a launching point for characterizing specific stromal and epithelial cell populations and determining how they participate in LUT development in male and female mice.

RESULTS

Expression patterns of 71 mRNAs were screened by ISH to identify selective tissue sub-compartment markers in 17 dpc male and female fetal mouse LUT. The screen included the following tissue compartments: bladder neck, pelvic urethra (defined in this study as the urethra spanning the bladder neck and the body wall, including the UGS and, in males, prostatic buds), caudal Wolffian duct (including seminal vesicle and ejaculatory duct) and caudal MÜllerian duct (including upper vagina, and lower vagina, also known as MÜllerian vagina and sinus vagina, respectively). The pattern of each mRNA was assessed in three replicate male and female LUTs and was anchored by its relative location to two tissue compartments: LUT epithelium (marked by cadherin 1 immunofluorescent staining and defined in Figs. 1 and 4) and LUT smooth muscle (marked by alpha 2 actin

immunofluorescent staining and defined in Fig. 5). Replicate male and female tissue sections were processed as a single experimental unit to allow for qualitative comparisons among biological replicates and between males and females. mRNA expression patterns that were reproduced across all male or female replicate sections were annotated using anatomical ontology terms from the Edinburgh Mouse Atlas Project (EMAP) (Burger et al., 2004). In some cases, existing EMAP anatomical ontology terms for 17 dpc mice were insufficient to describe specialized mRNA expression patterns and more specific anatomical terms were assigned. An annotated summary of LUT gene expression is provided in Supplemental Table 1 and additional ISH images are available at gudmap.org. Some of the mouse LUT tissue compartment markers reported in this manuscript have been reported previously in male, female, or both sexes. These mRNA markers are also included in this manuscript to ensure complete coverage of all identified LUT sub-compartments.

Selective labeling of fetal mouse basal, intermediate, and superficial urothelium with Krt14, Upk1b *and* Kremen1 *mRNAs*

In adult mice, a specialized transitional epithelium, or urothelium, lines the ureter, bladder, and urethra and is subdivided into basal, intermediate, and superficial layers. This subdivision occurs early in fetal bladder development (Castillo-Martin et al., 2010) but there is conflicting evidence about whether it also occurs early in fetal pelvic urethra development.

ISH was used to assess patterns of two mRNAs used previously to distinguish basal from intermediate/superficial urothelium in bladder: keratin 14 (*Krt14*) and uroplakin 1b (*Upk1b*), respectively. After ISH staining was completed, the entire LUT epithelium was co-stained by immunofluorescence with an anti-cadherin 1 antibody to localize *Krt14* and *Upk1b* to specific epithelial cell populations.

ISH revealed at least two distinct urothelial layers in 17 dpc male and female pelvic urethra. Basal urothelium was the deepest epithelial layer and was selectively marked by *Krt14* mRNA. *Krt14* was observed in a thin band of urothelium, 2-3 cell layers thick, located adjacent to the basement membrane that divides urothelium and stroma. *Krt14* mRNA marked basal urothelium along the entire caudal-cranial axis of the male and female pelvic urethra (Fig. 1A-B) and marked male prostatic bud and ejaculatory duct epithelium and female lower vagina epithelium (Fig. 1A-B). Interestingly, *Krt14* mRNA was not detected in the most cranial bladder basal urothelial cells at 17 dpc (the bladder apex, results not shown). Intermediate and superficial urothelial layers were marked by *Upk1b* (Fig. 1C-D). *Upk1b* mRNA was not observed in prostatic bud epithelium but was in ejaculatory duct epithelium and lower vagina epithelium. We screened 17 dpc pelvic urethra for mRNA markers that are known to be expressed selectively in superficial urothelium of adult bladder, including *Krt7*, *Krt20*, and *Upk3a* (Veranic et al., 2004). While all of these markers were present in fetal bladder urothelium, they were either absent from or were not selectively expressed in urethral superficial urothelium (results not shown). Thus, it is possible superficial urothelium in developing urethra versus adult bladder is marked by a unique set of mRNAs of which we are unaware. The fact that at least one mRNA, kringle containing transmembrane protein 1 (*Kremen1*), was present in basal and intermediate urothelium and was not detected in superficial urothelium of the urethra (Fig. 1E-F) provides evidence that a discrete superficial urothelial cell population exists in the 17 dpc mouse urethra.

Our observation that *Krt14* mRNA selectively marks urethral basal urothelium conflicts with a previous report of KRT14 protein marking all fetal urethral urothelial cells (Wang et al., 2001). It is necessary to address these conflicting results because in mature prostate, some basal epithelial cells exhibit progenitor cell-like characteristics (Lawson et al., 2007) and it

has been suggested that prostate progenitor cells are concentrated in fetal male UGS urothelium (Blum et al., 2010). Therefore, selective basal urothelial cell markers are likely to be useful research tools because they may enrich for fetal prostate progenitor cells.

We assessed whether the pattern of KRT14 protein expression matches the *Krt14* mRNA expression pattern observed in this study and matches the pattern of another known basal urothelial marker, transformation-related protein 63 (TRP63) (Signoretti et al., 2000). Immunofluorescent labeling of 17 dpc male and female mouse LUT sagittal sections was used to assess the location of KRT14 and TRP63 proteins. KRT14 was detected as early as 15 dpc (results not shown) and was present at 17 dpc in urethra urothelium and in trigone bladder urothelium but not other regions of the bladder (Fig. 2A-B). TRP63 staining was observed in a thicker band of urethra urothelium (5-6 cell layers thick) compared to KRT14 (2-3 cell layers thick) and, unlike KRT14, extended into the cranial bladder regions, including the fundus (Figure 2A-B). Although nuclear TRP63 staining was present in all KRT14-positive cells, it was also present in some KRT14-negative urothelial cells (Fig. 2A-B, yellow arrowheads). Thus, our data support the idea that *Krt14* mRNA and protein are specific markers of pelvic urethra basal urothelium in the 17 dpc mouse. Our results also indicate TRP63 is not a specific basal urothelial cell marker in pelvic urethra because it is present in $KRT14^{+}$ basal urothelial cells as well as $KRT14^{-}$ intermediate urothelial cells.

Wnt10b mRNA selectively labels fetal mouse prostate epithelium

Prostatic buds are present in male fetal mouse UGS as early as 16 dpc (Lin et al., 2003) and NK-3 transcription factor, locus 1 (*Nkx3-1*) is generally considered the most specific and earliest stage marker of prostate ductal identity. *Nkx3-1* mRNA is also present in non-urogenital tissues at 16 dpc, including the tooth bud, hair follicle, nasopharyngeal epithelium, and portions of the central nervous system (Tanaka et al., 1999). During male LUT development, *Nkx3-1* marks both prostatic buds and urethral gland buds that appose and are possibly intermixed with prostatic buds (Sciavolino et al., 1997; Allgeier et al., 2010). Therefore, a more specific fetal prostatic bud marker is needed to distinguish prostatic from urethral gland buds. We identified wingless-related MMTV integration site 10B (*Wnt10b*) as a specific prostatic bud marker in the 17 dpc male LUT (Fig. 3A). *Wnt10b* mRNA was present in ventral, anterior, and dorsolateral prostatic buds at 17 dpc but was not detected in ejaculatory duct or other epithelial structures within the male LUT. *Wnt10b* was not detected in most 17 dpc female mouse LUT structures. However, weak *Wnt10b* expression was observed in a small sub-population of basal urothelial cells in the dorsal aspect of the urethra (Fig. 3B).

Wnt10b and *Nkx3-1* mRNA expression were compared to determine whether *Wnt10b* marks prostatic buds more specifically than *Nkx3-1* in postnatal day (P) 0 male LUT, the stage when the full complement of prostatic and urethral gland buds are present in the male mouse fetus (Lin et al., 2003). *Wnt10b* and *Nkx3-1* mRNA expression patterns were different in P0 male mouse LUT (Fig. 3C-D). Although both mRNAs were detected in prostatic buds, *Wnt10b* mRNA was restricted to distal bud tips while *Nkx3-1* was present in distal and medial prostatic bud segments. Most notably, *Wnt10b* was not detected in caudal pelvic urethra where small urethral gland bud formation has initiated, while *Nkx3-1* was present in these structures (Timms et al., 1994; Lin et al., 2003). Therefore, compared to *Nkx3-1*, *Wnt10b* appears to be a specific marker of prostate epithelium in P0 male LUT.

The mouse prostate forms four lobes: ventral, dorsal, lateral, and anterior. There is strong evidence supporting the hypothesis that these lobes are patterned by ventral, dorsal, lateral, and anterior stroma, respectively, during fetal development (Hayashi et al., 1993; Timms et al., 1995; Ko et al., 2004). For the most part, we did not observe mRNAs that could distinguish between ventral, dorsal, lateral, or anterior prostatic bud epithelium. The one

exception was bone morphogenetic protein 2 (*Bmp2*), which was present in ventral prostatic bud epithelium but not detected in dorsal, lateral, or anterior prostatic bud epithelium (results not shown). *Bmp2* was also present in urethral lamina propria of both sexes, and in mesenchyme of ejaculatory duct, seminal vesicle, and upper and lower vagina.

Selective mRNA markers of MÜllerian and Wolffian duct compartments in the fetal mouse LUT

Selective markers of MÜllerian and Wolffian ducts in 17 dpc mice would not only be useful tools for understanding development of seminal vesicle, uterus and vagina, but they would also serve as a means to exclude these tissues when studying morphogenesis of other LUT structures, such as urethra and prostate. We identified anti-MÜllerian hormone receptor 2 (*Amhr2*) mRNA as a marker of vaginal mesenchyme in 17 dpc female LUT (Fig. 4B). Weak *Amhr2* expression was detected in urethra urothelium and muscularis propria of the 17 dpc male and female LUT (Fig. 4A-B). *Amhr2* was not detected in vaginal epithelium (Fig. 4B).

Homeobox b7 and paired box 2 have been used previously to identify MÜllerian and Wolffian duct epithelium in early stage mouse embryos (Dressler et al., 1990; Kress et al., 1990; Torres et al., 1995). In this study, additional selective mRNA markers for vaginal epithelium were identified and subdivided the vagina into epithelium of the upper and lower vagina (also known as the sinus vagina or sinovaginal bulb). *Wnt7a* had been described previously as a marker of MÜllerian duct epithelium in 17 dpc mice (Miller and Sassoon, 1998). In our study, it was not detected in most structures of the 17 dpc male LUT (Fig. 4C), with the exception of ductus deferens epithelium (results not shown). *Wnt7a* was present in upper vagina epithelium (Fig. 4D). It was not detected in lower vagina (sinus vagina), nor was it observed in urethral urothelium (Fig. 4D). While we did not identify a specific marker of lower vagina epithelium, many mRNA markers of basal urothelium were present in lower vagina and absent in upper vagina (Supplemental Table 1). One example is *Krt14* mRNA (Fig. 1B).

We observed selective expression of *Wnt9b* in seminal vesicle epithelium of 17 dpc males (Fig. 4E). *Wnt9b* was not detected in ejaculatory duct epithelium or in urethra urothelium of 17 dpc males and was not detected in any 17 dpc female LUT structures (Fig. 4F). We also identified cellular retinoic acid binding protein I (*Crabp1*) as a selective marker of seminal vesicle and ejaculatory duct mesenchyme (Fig. 4G). *Crabp1* was present in mesenchyme and smooth muscle of the seminal vesicle and ejaculatory duct. *Crabp1* was also present in vaginal mesenchyme and vaginal smooth muscle in 17 dpc females, as well as in lamina propria of the ventral urethra (Fig. 4H).

Selective mRNA markers of fetal mouse urethral stroma

UGS stroma plays a key role in prostate ductal morphogenesis. About one-third of urethral stromal cells in the UGS region are androgen receptor (AR) protein positive (unpublished observations) but it is unclear whether all or only a fraction of them synthesize the AR-responsive transcripts that are needed for prostate development. We used molecular markers to define urethral stromal sub-compartments as a first step towards the long term goal of determining which stromal compartments are needed for prostate development.

Adult mouse pelvic urethra is lined by lamina propria—a multi-cellular layer of loose connective tissue supporting a glandular epithelium. The mRNA for snail homolog 1 (*Snai1*) was selectively expressed in stromal cells of the 17 dpc male and female LUT lamina propria (Fig. 5A-B). The inner boundary of *Snai1* expression was the basement membrane of the urothelium while the outer boundary was muscularis mucosa, which was marked by a

thin band of ACTA2-protein positive muscle cells (Fig. 5A-B). *Snai1* was more abundant in male versus female urethral lamina propria.

The submucosal compartment of fetal mouse urethra was defined as a compartment of stroma that was bounded internally by a thin ACTA2-protein-positive muscularis mucosa and externally by thick ACTA2-positive muscularis propria. Although we were unable to identify a specific marker of submucosa mesenchyme (Fig. 5C-D), several mRNAs were present in both submucosa and lamina propria compartments (Table 1). An example is forkhead box F1a (*Foxf1a*) mRNA. ACTA2-positive muscularis mucosa divided *Foxf1a* expression into urethral lamina propria and submucosa compartments of 17 dpc male and female (Fig. 5C-D). *Foxf1a* also extended into the mesenchymal stroma of ejaculatory duct and vagina.

Muscularis propria is a thick smooth muscle layer external to urethral submucosa and has been defined previously in rat (Thomson et al., 2002) and mouse (Vezina et al., 2008) by smooth muscle alpha actin (ACTA2) expression. We found *Acta2* mRNA to be expressed in muscularis propria but also in muscularis mucosa of 17 dpc male and female as well as in smooth muscle of the vagina (Fig. 5E-F).

External to ACTA2-positive muscularis propria of the urethra, male and female urethral stroma contains three clusters of condensed mesenchyme that are centered on the midline of the left-right urethral axis and are visible in hematoxylin and eosin stained sections of 17 dpc mouse LUT (Fig. 6A-B). The arrangement of mesenchymal cells in each condensate showed a distinct swirl pattern. One of these condensed mesenchyme regions, the ventral mesenchymal pad (VMP), was identified initially in the rat because it was sufficient for instructing prostate differentiation in the presence of androgens (Timms et al., 1995). The VMP was subsequently shown to be a rich source of fibroblast growth factor 10 (FGF10) protein in rat (Thomson and Cunha, 1999) and mouse (Vezina et al., 2009). We assessed the pattern of *Fgf10* mRNA in 17 dpc male and female mouse LUT sagittal sections. Three clusters of *Fgf10* mRNA-positive mesenchymal pad mesenchyme were located external to the ACTA2-positive muscularis mucosa (Fig. 6C-D) and were present in male and female LUT in anatomical positions that were similar to the mesenchymal condensates shown in Fig. 6A-B. Mesenchymal pads in female urethra were smaller and more elongated than in the male urethra. Since the VMP is positioned near the origin of ventral prostatic ducts, we designated the other mesenchymal condensates as anterior mesenchymal pad (AMP) and dorsal mesenchymal pad (DMP) according to convention. These terms reflect the fact that AMP and DMP are positioned near the origins of anterior and dorsal prostatic bud formation in males (Fig. 6A-B). *Fgf10* was most prominent in the mesenchymal pads but was also observed in non-mesenchymal pad stroma, specifically in smooth muscle of vagina and ejaculatory duct and in a sub-population of urethral submucosa (Fig. 6C-D). Note that, while the dorsal mesenchymal pad is not present in the female LUT section shown in Fig. 6, it was present in adjacent tissue sections (results not shown).

There is some specificity with regard to mRNA expression in the mesenchymal pads. Although we were unable to identify mRNAs that selectively marked AMP or DMP, we did identify sex comb on midleg homolog 1 (*Scmh1*) as a specific VMP marker in 17 dpc male and female mouse LUT (Fig. 6E-F). *Scmh1* was absent from AMP, DMP, and most other LUT structures in 17 dpc males and females with the exception of ductus deferens mesenchyme (results not shown). Unlike other known selective VMP markers, such as *Fgf10* and signal peptide, CUB domain, EGF-like 1 (*Scube1*, not examined) (Vanpoucke et al., 2007), *Scmh1* was identified specifically in the VMP and not in muscularis propria or other smooth muscle of the LUT.

Selective labeling of vasculature and associated pericytes, macrophages, presumptive neural crest cells and interstitial cells of Cajal in the fetal mouse LUT

We sought to identify the location of vascular endothelium and associated pericytes during LUT development since these cell types have been linked to developmental processes in other organs (Benjamin et al., 1998; Lammert et al., 2001; Matsumoto et al., 2001; Duffield and Humphreys, 2011). A loose vascular plexus was evident in the stroma at 17 dpc. Vascular endothelial cells were marked by the mRNA for E26 avian leukemia oncogene 1, 5′ domain (*Ets1*, Fig. 7A-B) and were surrounded by presumptive pericytes that selectively expressed the pericyte marker (Mitchell et al., 2008) regulator of G-protein signaling 5 (*Rgs5*, Fig. 7C-D). Vascular endothelium and associated presumptive pericytes were observed along the entire caudal-cranial axis of the urethra and were also detected in stroma surrounding vaginal epithelium and seminal vesicle and ejaculatory duct epithelium. While *Rgs5* mRNA selectively marked pericytes in LUT stroma, it was not detected in all of the locations where *Ets1* marked vascular endothelium. Furthermore, *Rgs5* also marked a sub-population of non-pericyte basal and intermediate urothelial cells.

There is increasing evidence that macrophages play an important role in tubular development. The process of tubular repair after renal ischemia reperfusion injury has been linked to a reactivation of developmental signaling molecules and macrophages were recently identified as a source of one of these molecules (Lin et al., 2010). We identified presumptive macrophages in lamina propria marked by a known macrophage/monocyte lineage marker (O'Reilly et al., 2004), EGF-like module containing, mucin-like, hormone receptor-like sequence 1 *(Emr1*, Fig. 8A-B). *Emr1*-positive cells were also concentrated in vaginal epithelium and in mesenchyme located at the tips of developing seminal vesicles. The presence of macrophages in these regions was confirmed in hematoxylin and eosin-stained tissue sections (not shown).

We next assessed the expression pattern of *Sox10*, a marker of presumptive neural crest-derived cells (Southard-Smith et al., 1998). Neural crest derivatives are known to give rise to the paired major pelvic ganglia cells located near the lateral bounds of the adult mouse LUT (Durbec et al., 1996). It is also possible, though controversial, that neural crest cells give rise to neuroendocrine cells of the prostate (Aumuller et al., 2001; Goldstein et al., 2008). *Sox10* mRNA-positive cells were not abundant but were observed throughout urethral stroma (Fig. 8C-D). *Sox10*$^+$ cells were clustered cranial to the anterior prostatic budding zone, between the AMP and bladder (Fig. 8C). *Sox10*$^+$ cell clusters were also located near the caudal boundary of the ventral mesenchymal pad and in the muscularis propria of the urethra. It is important to note that *Sox10* is very abundant in pelvic ganglia, located on the lateral aspects of the developing LUT (Southard-Smith et al., 1998), but these cells are not visible in the mid-sagittal cut LUT sections used in this study (results not shown).

ICC are electrical pacemaker cells located within the muscularis propria of the gastrointestinal tract (Thuneberg, 1982; Thuneberg et al., 1982). They are derived from a mesenchymal precursor (Lecoin et al., 1996; Young et al., 1996) prior to birth (Ward et al., 1997) and are required for normal rhythmic contractility of gut (Ward et al., 1994). ICC, identified by kit oncogene (KIT) expression, have also been identified in sub-compartments of adult LUT including rabbit urethra (Sergeant et al., 2000), rat ductus deferens (Burton et al., 2000), human vagina (Shafik et al., 2005), guinea pig ureter (Klemm et al., 1999) and prostate (Exintaris et al., 2002). We examined the expression of *Kit* mRNA in fetal mice to identify putative ICC cells in the developing LUT, where rhythmic contractility is also known to exist (Cunha, 1973). Individual *Kit* mRNA-positive cells (white arrowheads) were identified in a thin band of muscularis propria of the urethra from the bladder neck to the body wall. Non-ICC *Kit* mRNA-positive urothelial cells were also identified in intermediate

urothelium of the UGS, which may be due to the fact that our probe recognizes both transcript variants of this gene.

A selective marker of androgen receptor-responsive transcription is present in male urethral lamina propria and ejaculatory duct mesenchyme

It has been known for over thirty-three years that prostate development is initiated in fetal males by ARs in UGS mesenchyme (Cunha and Lung, 1978) and it has been proposed that AR-responsive target genes called 'andromedins' are the key paracrine signals that initiate prostate development. Yet, while a variety of mesenchymal factors have been shown to be required for prostate development (Thomson, 2008), none are capable of activating prostate development in the absence of functional AR signaling. One reason that these signals have eluded us is that they may be expressed in select stromal cell populations of the fetal prostate at discrete gestational stages, causing them to be diluted by other stroma in gene expression profiling studies.

We assessed the pattern of steroid 5 alpha-reductase 2 (*Srd5a2*) mRNA to pinpoint the stromal cell compartment where AR signaling is activated in male mouse LUT. *Srd5a2* requires androgens and functional ARs for its transcription in fetal mouse LUT (Supplemental Fig. 1; (Matsui et al., 2002). In 17 dpc male LUT, *Srd5a2* mRNA was present in urethral lamina propria, peri-prostatic mesenchyme, and seminal vesicle and ejaculatory duct mesenchyme (Fig. 9A). In female 17 dpc LUT, *Srd5a2* mRNA was not detected in lamina propria but it was present in a compartment of mesenchyme located on the dorsal aspect of the lower vagina (Fig. 9B), approximately in the same position as the Wolffian duct prior to its regression. There was a relatively close association between the intensity of *Srd5a2* mRNA staining in the male and female LUT and the density of AR-positive mesenchymal cell nuclei (Fig. 9C-D). Therefore, *Srd5a2* mRNA is a useful tool for marking male LUT stroma where androgen receptors are active.

Subdivision of fetal mouse LUT ontology into dorsal and ventral components

Some of the transcripts assessed in our study demonstrated striking dorsoventral differences in expression, and these transcripts may provide insight into mechanisms of LUT dorsoventral patterning. GATA binding protein 2 (*Gata2*) is an example of an mRNA with a dorsalized expression pattern in the pelvic urethra. *Gata2* was present in mesenchyme, epithelium, and neural-crest derived cells of the dorsal aspect of the 17 dpc male and female urethra but was not detected along the right-left midline of the ventral urethra at this stage (Fig. 10A-B). Frizzled related protein (*Frzb*, also known as secreted frizzled related protein 3) is an example of an mRNA with a ventralized expression pattern in the pelvic urethra. *Frzb* was more abundant in ventral versus dorsal lamina propria of the UGS portion of the pelvic urethra, especially in male ventral versus anterior prostatic region and the equivalent region in female (Fig. 10C-D). Because dorsoventral gene expression gradients may reveal important mechanisms of pattern formation during LUT morphogenesis, all urethra ontology terms in the GUDMAP database were subdivided to include dorsal and ventral compartments. A schematic diagram of all LUT sub-compartments identified by this study is shown in Fig. 11.

DISCUSSION

This manuscript summarizes the results of an ISH screen, conducted in collaboration with GUDMAP, to identify specific LUT tissue compartment markers and synthesize a high-resolution molecular map of fetal mouse LUT anatomy. A major contribution of this work is that it defines several tissue sub-compartments of 17 dpc fetal mouse LUT that have not

been described previously, to our knowledge. These results will facilitate high resolution annotation of future gene and protein expression results in fetal mouse LUT.

The approximate position and boundaries of LUT tissue compartments described in this study are shown schematically in Fig. 11. Eight epithelial compartments are described for the 17 dpc male and female LUT. These compartments, along with the most selective mRNA markers that identify them, include: basal *(Krt14*$^{+}$), intermediate (*Kremen1*$^{+}$;*Upk1b*$^{+}$) and superficial urothelium (*Kremen1*$^{-}$;*Upk1b*$^{+}$), seminal vesicle epithelium (*Wnt9b*$^{+}$), ejaculatory duct epithelium (*Krt14*$^{+}$), prostatic bud epithelium (*Wnt10b*$^{+}$), lower vagina epithelium (*Krt14*$^{+}$), and upper vagina epithelium (*Wnt7a*$^{+}$). Sixteen stromal compartments are described for 17 dpc male and female LUT. These compartments and their selective mRNA markers include: lamina propria of urethra (*Snai1*$^{+}$), muscularis mucosa of urethra (*Acta2*$^{+}$), submucosa of urethra (*Foxf1a*$^{+}$;*Snai1*$^{-}$), muscularis propria of urethra (*Acta2*$^{+}$), VMP (*Scmh1*$^{+}$;*Fgf10*$^{+}$), AMP (*Scmh1*$^{-}$;*Fgf10*$^{+}$), and DMP (*Scmh1*$^{-}$;*Fgf10*$^{+}$), vascular endothelium of urethra (*Ets1*$^{+}$), presumptive vascular pericytes of urethra (*Rgs5*$^{+}$), presumptive macrophages of urethra (*Emr1*$^{+}$), presumptive neural crest-derived cells of urethra *(Sox10*$^{+}$), presumptive ICC of urethra (*Kit*$^{+}$), mesenchyme of upper and lower vagina (*Acta2*$^{+}$), smooth muscle of upper and lower vagina, smooth muscle of ejaculatory duct (*Acta2*$^{+}$;*Crabp1*$^{+}$), mesenchyme of the ejaculatory duct (*Crabp1*$^{+}$). We also describe the pattern of at least one androgen-responsive mRNA in the urethra, *Srd5a2*$^{+}$, which was noticeably more abundant in male versus female urethral lamina propria and was also concentrated in ejaculatory duct mesenchyme.

A limitation of this study is that mRNAs identified as selective compartment markers were defined as such by comparing their expression to other structures in isolated mouse LUT tissues. While these are useful markers for identifying micro-anatomical tissue compartments in the LUT, it is highly unlikely that these mRNAs are present only in LUT. Furthermore, the pattern of mRNA markers described in this manuscript has not been examined across all stages of mouse LUT development, and has not been investigated in the developing LUT of other species. Such studies are needed to extend the utility of this molecular anatomy resource.

There are several ways that these results will improve LUT development research. First, they reveal many differences in 17 dpc male versus female LUT anatomy. Aside from obvious anatomical sexual dimorphism (MÜllerian and Wolffian duct-derived structures), the mesenchymal pads of male LUT are larger than female, the lamina propria and submucosa layers of the urethra are thicker in male than female, urethral gland buds are larger in male than female, and the muscularis propria layer is thicker in female than male. Also, there appear to be differences in the distribution and quantity of presumptive macrophages in male versus female LUT. These collective differences are noteworthy because many investigators have made male versus female comparisons of UGS stromal mRNA and protein abundance in order to identify androgen-responsive genes in the male. Such comparisons are likely to be confounded by sexually dimorphic anatomy in this region and may be misleading if unaccompanied by information about gene expression patterns.

Results from this study are likely to refine several methodological approaches used currently for LUT research. An enzymatic digestion and mechanical separation technique (Cunha and Lung, 1978) is frequently used to obtain purified urethral epithelium and stromal cell populations for gene expression analyses or for morphogenesis studies. Most of these studies confirm purity of separated epithelium and mesenchyme by demonstrating the presence or absence of epithelial or mesenchymal-selective mRNAs. The use of some mRNAs, such as *Acta2*, to confirm the purity of these tissue preparations would be uninformative because *Acta2* mRNA-positive cells reside several cells away from the mesenchymal-epithelial

interface and are not likely to reveal whether cross-contamination exists. We have identified differentially expressed mRNAs in epithelial and stromal cell populations residing on or near the urethral basement membrane. Based on our results, it would be prudent to confirm in future studies that purified urethral stroma is free of *Krt14*$^{+}$ basal cell contamination and that purified urothelium is free of *Snai1*$^{+}$ lamina propria contamination.

The identification of *Wnt10b* mRNA as an early stage and specific marker of prostate ductal identity is likely to have many impacts in prostate biology research. An immediate application for this result is that *Wnt10b* ISH could be used to track the quantity and size of prostatic buds formed during prostate development *in utero* or *in vitro*. Because prostatic bud formation is a common endpoint for assessing prostate morphogenetic mechanisms and for testing whether pharmacological agents and other xenobiotics inappropriately influence prostate development, several methods have been developed to visualize the fetal prostate in three dimensions and enumerate prostatic buds. These methods including scanning electron microscopy of purified urethral epithelium (Lin et al., 2003), computer-assisted serial reconstruction of prostate serial sections (Timms et al., 1994), and ISH staining of whole-mount LUT for the prostate selective marker *Nkx3-1* (Thomsen et al., 2008). The first two methods are time consuming and none of the methods can differentiate epithelial buds that will elongate into prostate ducts from those that will become urethral glands. *Wnt10b* mRNA selectively marks prostatic buds but not urethral gland buds. Thus, enumeration of *Wnt10b* mRNA–positive prostatic buds in ISH stained tissues is a means to accurately and specifically quantify prostatic buds in male LUTs grown *in utero* or in organ culture.

Wnt10b may also serve as an important resource for future mechanistic studies of prostate development and for marking epithelial buds in other organs that undergo budding and branching morphogenesis. *Wnt10b* has already been identified in some of these organs, including hair follicles (Reddy et al., 2001), dental placodes (Liu et al., 2008) and taste papillae (Suzuki et al., 2010). The synthesis of a *Wnt10b-Cre*/reporter mouse would be a useful tool for tracking the lineage of these cells during subsequent phases of prostate development, such as branching morphogenesis and cytodifferentiation. Such a mouse could also be used to compare gene expression profiles of *Wnt10b*$^{+}$ basal epithelial cells concentrated in invasive growth areas at the tips of prostatic buds versus *Wnt4*$^{+}$ basal epithelial cells located in the base of prostatic buds where ductal lumenization and cytodifferentiation begin (Hayward et al., 1996).

In the female reproductive tract, results of this study shed light on a long standing controversy over whether vaginal epithelium in the fetus is entirely derived from MÜllerian duct epithelium or whether urethral epithelium also contributes to this fetal structure. Our results support a recent cell lineage analysis study that reveals UGS epithelium as an origin of the lower vagina in fetal females (Kurita, 2010). In our study, nearly all mRNAs present in basal urothelium were also present in lower vagina. Likewise, nearly all mRNAs exclusively present in upper vagina were excluded from urethral urothelium and lower vagina. These results are consistent with the notion that lower vagina of the fetal mouse fetus is derived from UGS epithelium as suggested by Kurita (2010). A limitation of our results is that they do not shed light on whether, in sexually mature mice, any component of adult vagina is derived from urethral epithelium, an idea supported by the recent study of Kurita (2010).

Results of this study reveal the need for further refinement of our knowledge about which urethral stromal and epithelial compartments are required for androgen-dependent induction of prostatic bud formation. It is known that at least two purified adult mouse prostate epithelial cell populations are enriched with progenitor cells and are capable of giving rise to mature prostate ducts when combined with 16 dpc male urethral mesenchyme (Leong et al.,

2008; Wang et al., 2009). While fetal mouse urethral and adult bladder urothelial cells are also capable of forming prostate under these conditions (Cunha and Chung, 1981; Li et al., 2009), it is unclear which urothelial cell population (basal, intermediate, or superficial) is responsible. Likewise, it is unclear which of the urethral stromal compartments provide the key inductive signals needed for prostate development. The mRNA compartment markers identified in this study can be used to refine and further purify fetal prostate cell populations in order to isolate progenitor cells giving rise to prostate and the stromal sources of inductive signals that activate these progenitors.

EXPERIMENTAL PROCEDURES

Animals

C57BL/6J mice (Jackson Laboratory, Bar Harbor, ME) were housed in clear plastic cages containing corn cob bedding and maintained on a 12 hr light and dark cycle at 25±5°C and 20-50% relative humidity. Feed (Diet 2019 for males and Diet 7002 for pregnant females, Harlan Teklad, Madison, WI) and water were available *ad libitum*. All procedures were approved by the University of Wisconsin Animal Care and Use Committee and conducted in accordance with the NIH Guide for the Care and Use of Laboratory Animals. To obtain timed-pregnant dams, female mice were paired overnight with males. The next day was considered 0 dpc. Dams were euthanized by CO_2 asphyxiation and fetuses were maintained in Hank's Balanced Salt Solution prior to dissection.

In Situ *Hybridization (ISH)*

Detailed protocols are available at www.gudmap.org and are described in a companion publication (Abler et al., 2011). Fetal male and female mouse lower LUT tissues were fixed overnight at 4°C in phosphate buffered saline containing 4% paraformaldehyde. Tissues were dehydrated in 100% methanol for archival storage at -20°C for up to two years and rehydrated prior to sectioning. Tissue sectioning and ISH were conducted as described previously (Abler et al., 2011). Primer sequences used to generate probe templates are provided in Supplementary Table 2, except for *Fgf10* (Bellusci et al., 1997) and *Snai1* (Locascio et al., 2002), which are plasmid-based probes. BM Purple was used as an alkaline phosphatase chromagen for detection of digoxigenin-labeled riboprobes. The staining pattern for each hybridized riboprobe was assessed in at least two LUT sections / mouse fetus and at least three litter-independent fetuses. Information about the PCR-generated riboprobes used in this study is available in Supplemental Table 2.

Immunofluorescent staining of paraffin sections

Tissues were fixed in 4% paraformaldehyde, dehydrated into methanol, infiltrated with paraffin, and cut into 5 μm sections. Sections were deparaffinized in xylene, hydrated, and boiled in 10 mM sodium citrate (pH 6.0) for 20 min. Tissues were washed with a solution containing 25 mM Tris-HCl, pH 7.5, 140 mM NaCl, 2.7 mM KCl, and 0.1% Tween-20 (TBSTw) and non-specific binding sites were blocked for 1 hr in TBSTw containing 1% Blocking Reagent (Roche Diagnostics), 5% normal goat sera, and 1% bovine serum albumin fraction 5 (RGBTw). Tissues were incubated overnight at 4°C with primary antibodies diluted in RGBTw as follows: 1:250 rabbit anti-AR (Santa Cruz Biotechnology, Santa Cruz, CA), 1:250 rabbit anti-CDH1 (Cell Signaling Technologies, Beverly MA), 1:50 mouse anti-KRT14 (Thermo Fisher Scientific, Waltham MA), 1:250 mouse anti-TRP63 (Santa Cruz Biotechnology). After several washes with TBSTw, tissues were incubated for 1 hr with RGBT containing 1:250 diluted fluorescent secondary antibodies (Dylight 488- and 405-conjugated goat anti-mouse IgG, Dylight 546-counjugated goat anti-rabbit IgG, Jackson Immunoresearch (West Grove, PA). For sections that were stained with two primary antibodies from the same host species, unlabeled secondary antibodies (goat anti-mouse or

goat anti-rabbit IgG, Jackson Immunoresearch) were used to block antigenic sites prior to introducing the second primary antibody. Labeled tissue sections were counterstained with 4′,6-diamidino-2-phenylindole dilactate and mounted in anti-fade media (phosphate-buffered saline containing 80% glycerol and 0.2% n-propyl gallate). *Immunofluorescent staining of ISH-stained sections*. ISH stained tissue sections were fixed overnight in 4% PFA and bleached with TBSTw containing 6% hydrogen peroxide. Tissues were blocked for 1 h in RGBTw and then incubated overnight at 4°C in RGBTw containing rabbit anti-CDH1 (1:500, Cell Signaling Technologies) and mouse anti-ACTA2 (1:300, Leica Microsystems, Bannockburn, IL). Tissues were stained with secondary antibodies (1:500 Dylight 488-goat anti-mouse IgG, 1:500 Dylight 546- counjugated goat anti-rabbit IgG, Jackson Immunoresearch) and mounted in anti-fade media. Brightfield and fluorescent images were captured using an Eclipse E600 compound microscope (Nikon Instruments Inc., Melville, NY) and merged using NIS elements imaging software (Nikon Instruments Inc.)

Supplementary Material

Refer to Web version on PubMed Central for supplementary material.

Acknowledgments

The authors would like to thank Donald McCall and Charles Vezina for technical assistance and Dr. Stephen Mason for his suggestions during the preparation of this manuscript.

REFERENCES

Abler LL, Mehta V, Keil KP, Joshi PS, Flucus C-L, Hardin HA, Schmitz CT, Vezina CM. A high throughput in situ hybridization method to characterize mRNA expression patterns in the fetal mouse lower urogenital tract. J Vis Exp. 2011 In Press.

Allgeier SH, Lin TM, Moore RW, Vezina CM, Abler LL, Peterson RE. Androgenic regulation of ventral epithelial bud number and pattern in mouse urogenital sinus. Dev Dyn. 2010; 239:373–385. [PubMed: 19941349]

Aumuller G, Leonhardt M, Renneberg H, von Rahden B, Bjartell A, Abrahamsson PA. Semiquantitative morphology of human prostatic development and regional distribution of prostatic neuroendocrine cells. Prostate. 2001; 46:108–115. [PubMed: 11170138]

Bellusci S, Grindley J, Emoto H, Itoh N, Hogan BL. Fibroblast growth factor 10 (FGF10) and branching morphogenesis in the embryonic mouse lung. Development. 1997; 124:4867–4878. [PubMed: 9428423]

Benjamin LE, Hemo I, Keshet E. A plasticity window for blood vessel remodelling is defined by pericyte coverage of the preformed endothelial network and is regulated by PDGF-B and VEGF. Development. 1998; 125:1591–1598. [PubMed: 9521897]

Blum R, Gupta R, Burger PE, Ontiveros CS, Salm SN, Xiong X, Kamb A, Wesche H, Marshall L, Cutler G, Wang X, Zavadil J, Moscatelli D, Wilson EL. Molecular signatures of the primitive prostate stem cell niche reveal novel mesenchymal-epithelial signaling pathways. PLoS One. 2010:5.

Brunskill EW, Aronow BJ, Georgas K, Rumballe B, Valerius MT, Aronow J, Kaimal V, Jegga AG, Yu J, Grimmond S, McMahon AP, Patterson LT, Little MH, Potter SS. Atlas of gene expression in the developing kidney at microanatomic resolution. Dev Cell. 2008; 15:781–791. [PubMed: 19000842]

Burger A, Davidson D, Baldock R. Formalization of mouse embryo anatomy. Bioinformatics. 2004; 20:259–267. [PubMed: 14734318]

Burton LD, Housley GD, Salih SG, Jarlebark L, Christie DL, Greenwood D. P2×2 receptor expression by interstitial cells of Cajal in vas deferens implicated in semen emission. Auton Neurosci. 2000; 84:147–161. [PubMed: 11111847]

Castillo-Martin M, Domingo-Domenech J, Karni-Schmidt O, Matos T, Cordon-Cardo C. Molecular pathways of urothelial development and bladder tumorigenesis. Urol Oncol. 2010; 28:401–408. [PubMed: 20610278]

Cunha GR. Peristaltic contractions of the murine urogenital sinus. Anat Rec. 1973; 177:561–568. [PubMed: 4762730]

Cunha GR, Chung LW. Stromal-epithelial interactions--I. Induction of prostatic phenotype in urothelium of testicular feminized (Tfm/y) mice. J Steroid Biochem. 1981; 14:1317–1324. [PubMed: 6460136]

Cunha GR, Fujii H, Neubauer BL, Shannon JM, Sawyer L, Reese BA. Epithelial-mesenchymal interactions in prostatic development. I. morphological observations of prostatic induction by urogenital sinus mesenchyme in epithelium of the adult rodent urinary bladder. J Cell Biol. 1983; 96:1662–1670. [PubMed: 6853597]

Cunha GR, Lung B. The possible influence of temporal factors in androgenic responsiveness of urogenital tissue recombinants from wild-type and androgen-insensitive (*Tfm*) mice. J Exp Zool. 1978; 205:181–193. [PubMed: 681909]

Dressler GR, Deutsch U, Chowdhury K, Nornes HO, Gruss P. Pax2, a new murine paired-box-containing gene and its expression in the developing excretory system. Development. 1990; 109:787–795. [PubMed: 1977574]

Duffield JS, Humphreys BD. Origin of new cells in the adult kidney: results from genetic labeling techniques. Kidney Int. 2011; 79:494–501. [PubMed: 20861816]

Durbec PL, Larsson-Blomberg LB, Schuchardt A, Costantini F, Pachnis V. Common origin and developmental dependence on c-ret of subsets of enteric and sympathetic neuroblasts. Development. 1996; 122:349–358. [PubMed: 8565847]

Exintaris B, Klemm MF, Lang RJ. Spontaneous slow wave and contractile activity of the guinea pig prostate. J Urol. 2002; 168:315–322. [PubMed: 12050563]

Goldstein AS, Lawson DA, Cheng D, Sun W, Garraway IP, Witte ON. Trop2 identifies a subpopulation of murine and human prostate basal cells with stem cell characteristics. Proc Natl Acad Sci U S A. 2008; 105:20882–20887. [PubMed: 19088204]

Hayashi N, Cunha GR, Parker M. Permissive and instructive induction of adult rodent prostatic epithelium by heterotypic urogenital sinus mesenchyme. Epithelial Cell Biol. 1993; 2:66–78. [PubMed: 8353595]

Hayward SW, Baskin LS, Haughney PC, Cunha AR, Foster BA, Dahiya R, Prins GS, Cunha GR. Epithelial development in the rat ventral prostate, anterior prostate and seminal vesicle. Acta Anat (Basel). 1996; 155:81–93. [PubMed: 8828706]

Higgins SJ, Young P, Cunha GR. Induction of functional cytodifferentiation in the epithelium of tissue recombinants. II. Instructive induction of Wolffian duct epithelia by neonatal seminal vesicle mesenchyme. Development. 1989; 106:235–250. [PubMed: 2591313]

Klemm MF, Exintaris B, Lang RJ. Identification of the cells underlying pacemaker activity in the guinea-pig upper urinary tract. J Physiol. 1999; 519(Pt 3):867–884. [PubMed: 10457097]

Ko K, Moore RW, Peterson RE. Aryl hydrocarbon receptors in urogenital sinus mesenchyme mediate the inhibition of prostatic epithelial bud formation by 2,3,7,8-tetrachlorodibenzo-*p*-dioxin. Toxicol Appl Pharmacol. 2004; 196:149–155. [PubMed: 15050416]

Kress C, Vogels R, De Graaff W, Bonnerot C, Meijlink F, Nicolas JF, Deschamps J. Hox-2.3 upstream sequences mediate lacZ expression in intermediate mesoderm derivatives of transgenic mice. Development. 1990; 109:775–786. [PubMed: 1977573]

Kurita T. Developmental origin of vaginal epithelium. Differentiation. 2010; 80:99–105. [PubMed: 20638775]

Kurita T, Cooke PS, Cunha GR. Epithelial-stromal tissue interaction in paramesonephric (Mullerian) epithelial differentiation. Dev Biol. 2001; 240:194–211. [PubMed: 11784056]

Lammert E, Cleaver O, Melton D. Induction of pancreatic differentiation by signals from blood vessels. Science. 2001; 294:564–567. [PubMed: 11577200]

Lasnitzki I, Mizuno T. Prostatic induction: interaction of epithelium and mesenchyme from normal wild-type mice and androgen-insensitive mice with testicular feminization. J Endocrinol. 1980; 85:423–428. [PubMed: 7411008]

Lawson DA, Xin L, Lukacs RU, Cheng D, Witte ON. Isolation and functional characterization of murine prostate stem cells. Proc Natl Acad Sci U S A. 2007; 104:181–186. [PubMed: 17185413]

Lecoin L, Gabella G, Le Douarin N. Origin of the c-kit-positive interstitial cells in the avian bowel. Development. 1996; 122:725–733. [PubMed: 8631250]

Leong KG, Wang BE, Johnson L, Gao WQ. Generation of a prostate from a single adult stem cell. Nature. 2008; 456:804–808. [PubMed: 18946470]

Li X, Wang Y, Sharif-Afshar AR, Uwamariya C, Yi A, Ishii K, Hayward SW, Matusik RJ, Bhowmick NA. Urothelial transdifferentiation to prostate epithelia is mediated by paracrine TGF-beta signaling. Differentiation. 2009; 77:95–102. [PubMed: 19281768]

Lin SL, Li B, Rao S, Yeo EJ, Hudson TE, Nowlin BT, Pei H, Chen L, Zheng JJ, Carroll TJ, Pollard JW, McMahon AP, Lang RA, Duffield JS. Macrophage Wnt7b is critical for kidney repair and regeneration. Proc Natl Acad Sci U S A. 2010; 107:4194–4199. [PubMed: 20160075]

Lin TM, Rasmussen NT, Moore RW, Albrecht RM, Peterson RE. Region-specific inhibition of prostatic epithelial bud formation in the urogenital sinus of C57BL/6 mice exposed *in utero* to 2,3,7,8-tetrachlorodibenzo-*p*-dioxin. Toxicological Sciences. 2003; 76:171–181. [PubMed: 12944588]

Liu F, Chu EY, Watt B, Zhang Y, Gallant NM, Andl T, Yang SH, Lu MM, Piccolo S, Schmidt-Ullrich R, Taketo MM, Morrisey EE, Atit R, Dlugosz AA, Millar SE. Wnt/beta-catenin signaling directs multiple stages of tooth morphogenesis. Dev Biol. 2008; 313:210–224. [PubMed: 18022614]

Locascio A, Manzanares M, Blanco MJ, Nieto MA. Modularity and reshuffling of Snail and Slug expression during vertebrate evolution. Proc Natl Acad Sci U S A. 2002; 99:16841–16846. [PubMed: 12482931]

Matsui D, Sakari M, Sato T, Murayama A, Takada I, Kim M, Takeyama K, Kato S. Transcriptional regulation of the mouse steroid 5alpha-reductase type II gene by progesterone in brain. Nucleic Acids Res. 2002; 30:1387–1393. [PubMed: 11884637]

Matsumoto K, Yoshitomi H, Rossant J, Zaret KS. Liver organogenesis promoted by endothelial cells prior to vascular function. Science. 2001; 294:559–563. [PubMed: 11577199]

Miller C, Sassoon DA. Wnt-7a maintains appropriate uterine patterning during the development of the mouse female reproductive tract. Development. 1998; 125:3201–3211. [PubMed: 9671592]

Mitchell TS, Bradley J, Robinson GS, Shima DT, Ng YS. RGS5 expression is a quantitative measure of pericyte coverage of blood vessels. Angiogenesis. 2008; 11:141–151. [PubMed: 18038251]

O'Reilly D, Addley M, Quinn C, MacFarlane AJ, Gordon S, McKnight AJ, Greaves DR. Functional analysis of the murine Emr1 promoter identifies a novel purine-rich regulatory motif required for high-level gene expression in macrophages. Genomics. 2004; 84:1030–1040. [PubMed: 15533720]

Price JM, Donahoe PK, Ito Y, Hendren WH 3rd. Programmed cell death in the Mullerian duct induced by Mullerian inhibiting substance. Am J Anat. 1977; 149:353–375. [PubMed: 879051]

Reddy S, Andl T, Bagasra A, Lu MM, Epstein DJ, Morrisey EE, Millar SE. Characterization of Wnt gene expression in developing and postnatal hair follicles and identification of Wnt5a as a target of Sonic hedgehog in hair follicle morphogenesis. Mech Dev. 2001; 107:69–82. [PubMed: 11520664]

Sciavolino PJ, Abrams EW, Yang L, Austenberg LP, Shen MM, Abate-Shen C. Tissue-specific expression of murine Nkx3.1 in the male urogenital system. Dev Dyn. 1997; 209:127–138. [PubMed: 9142502]

Sergeant GP, Hollywood MA, McCloskey KD, Thornbury KD, McHale NG. Specialised pacemaking cells in the rabbit urethra. J Physiol. 2000; 526(Pt 2):359–366. [PubMed: 10896724]

Shafik A, El-Sibai O, Shafik I, Shafik AA. Immunohistochemical identification of the pacemaker cajal cells in the normal human vagina. Arch Gynecol Obstet. 2005; 272:13–16. [PubMed: 15834581]

Signoretti S, Waltregny D, Dilks J, Isaac B, Lin D, Garraway L, Yang A, Montironi R, McKeon F, Loda M. p63 is a prostate basal cell marker and is required for prostate development. Am J Pathol. 2000; 157:1769–1775. [PubMed: 11106548]

Southard-Smith EM, Kos L, Pavan WJ. Sox10 mutation disrupts neural crest development in Dom Hirschsprung mouse model. Nat Genet. 1998; 18:60–64. [PubMed: 9425902]

Suzuki Y, Ikeda K, Kawakami K. Regulatory role of Six1 in the development of taste papillae. Cell Tissue Res. 2010; 339:513–525. [PubMed: 20143239]

Tanaka M, Lyons GE, Izumo S. Expression of the Nkx3.1 homobox gene during pre and postnatal development. Mech Dev. 1999; 85:179–182. [PubMed: 10415359]

Thiagarajan RD, Rumballe BA, Lesieur E, Chiu HS, Taylor D, Tang DTP, Grimmond SM, Little MH. Identification of Anchor Genes during Kidney Development Defines Ontological Relationships, Molecular Subcompartments and Regulatory Pathways. PLoS One. 2011; 6:e17286. [PubMed: 21386911]

Thomsen MK, Butler CM, Shen MM, Swain A. Sox9 is required for prostate development. Dev Biol. 2008; 316:302–311. [PubMed: 18325490]

Thomson AA. Mesenchymal mechanisms in prostate organogenesis. Differentiation. 2008; 76:587–598. [PubMed: 18752494]

Thomson AA, Cunha GR. Prostatic growth and development are regulated by FGF10. Development. 1999; 126:3693–3701. [PubMed: 10409514]

Thomson AA, Timms BG, Barton L, Cunha GR, Grace OC. The role of smooth muscle in regulating prostatic induction. Development. 2002; 129:1905–1912. [PubMed: 11934856]

Thuneberg L. Interstitial cells of Cajal: intestinal pacemaker cells? Adv Anat Embryol Cell Biol. 1982; 71:1–130. [PubMed: 7090872]

Thuneberg L, Rumessen JJ, Mikkelsen HB. Interstitial cells of Cajal - an intestinal impulse generation and conduction system? Scand J Gastroenterol Suppl. 1982; 71:143–144. [PubMed: 6951268]

Timms BG, Lee CW, Aumuller G, Seitz J. Instructive induction of prostate growth and differentiation by a defined urogenital sinus mesenchyme. Microsc Res Tech. 1995; 30:319–332. [PubMed: 7606051]

Timms BG, Mohs TJ, Didio LJ. Ductal budding and branching patterns in the developing prostate. J Urol. 1994; 151:1427–1432. [PubMed: 8158800]

Tomaszewski J, Joseph A, Archambeault D, Yao HH. Essential roles of inhibin beta A in mouse epididymal coiling. Proc Natl Acad Sci U S A. 2007; 104:11322–11327. [PubMed: 17592132]

Torres M, Gomez-Pardo E, Dressler GR, Gruss P. Pax-2 controls multiple steps of urogenital development. Development. 1995; 121:4057–4065. [PubMed: 8575306]

Vanpoucke G, Orr B, Grace OC, Chan R, Ashley GR, Williams K, Franco OE, Hayward SW, Thomson AA. Transcriptional profiling of inductive mesenchyme to identify molecules involved in prostate development and disease. Genome Biol. 2007; 8:R213. [PubMed: 17922897]

Veranic P, Romih R, Jezernik K. What determines differentiation of urothelial umbrella cells? Eur J Cell Biol. 2004; 83:27–34. [PubMed: 15085953]

Vezina CM, Allgeier SH, Moore RW, Lin TM, Bemis JC, Hardin HA, Gasiewicz TA, Peterson RE. Dioxin causes ventral prostate agenesis by disrupting dorsoventral patterning in developing mouse prostate. Toxicol Sci. 2008; 106:488–496. [PubMed: 18779384]

Vezina CM, Hardin HA, Moore RW, Allgeier SH, Peterson RE. 2,3,7,8-Tetrachlorodibenzo-*p*-dioxin Inhibits Fibroblast Growth Factor 10-Induced Prostatic Bud Formation in Mouse Urogenital Sinus. Toxicol Sci. 2009; 113:198–206. [PubMed: 19805408]

Wang X, Kruithof-de Julio M, Economides KD, Walker D, Yu H, Halili MV, Hu YP, Price SM, Abate-Shen C, Shen MM. A luminal epithelial stem cell that is a cell of origin for prostate cancer. Nature. 2009; 461:495–500. [PubMed: 19741607]

Wang Y, Hayward S, Cao M, Thayer K, Cunha G. Cell differentiation lineage in the prostate. Differentiation. 2001; 68:270–279. [PubMed: 11776479]

Ward SM, Burns AJ, Torihashi S, Sanders KM. Mutation of the proto-oncogene c-kit blocks development of interstitial cells and electrical rhythmicity in murine intestine. J Physiol. 1994; 480(Pt 1):91–97. [PubMed: 7853230]

Ward SM, Harney SC, Bayguinov JR, McLaren GJ, Sanders KM. Development of electrical rhythmicity in the murine gastrointestinal tract is specifically encoded in the tunica muscularis. J Physiol. 1997; 505(Pt 1):241–258. [PubMed: 9409486]

Wilson JD, Griffin JE, Leshin M, George FW. Role of gonadal hormones in development of the sexual phenotypes. Hum Genet. 1981; 58:78–84. [PubMed: 6895207]

Young HM, Ciampoli D, Southwell BR, Newgreen DF. Origin of interstitial cells of Cajal in the mouse intestine. Dev Biol. 1996; 180:97–107. [PubMed: 8948577]

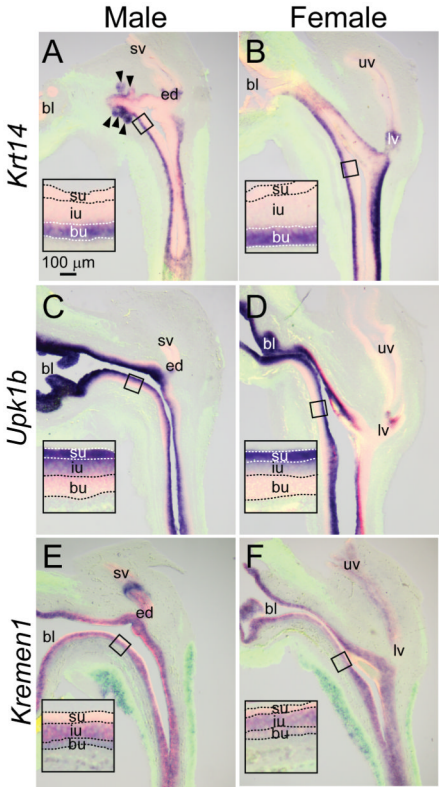

Fig. 1.

Selective mRNA markers of basal, intermediate, and superficial urothelial cell compartments in the 17 dpc mouse urethra. Near mid-sagittal sections (50 μm) of 17 dpc male and female LUT were stained by ISH to visualize mRNA expression (purple) of (**A-B**) the basal urothelial marker keratin 14 (*Krt14*), (**C-D**) the intermediate and superficial urothelial marker uroplakin 1b (*Upk1b*), and (**E-F**) the basal and intermediate urothelial marker kringle containing transmembrane protein 1 (*Kremen1*). Sections were then stained by immunofluorescence with an anti-smooth muscle actin alpha 2 (ACTA2) antibody that recognizes muscularis mucosa and muscularis propria (green) and an anti-cadherin 1 (CDH1) antibody that recognizes all urothelium (red). Inset images are magnified sections of urothelium that reveal the basal urothelium (bu), intermediate urothelium (iu), and superficial urothelium (su) sub-compartments. Results in each panel are representative of three males and three females. Abbreviations used are BL: bladder, ED: ejaculatory duct, LV: lower vagina, SV: seminal vesicle, UV: upper vagina. Arrowheads indicate prostatic buds. All images are of the same magnification.

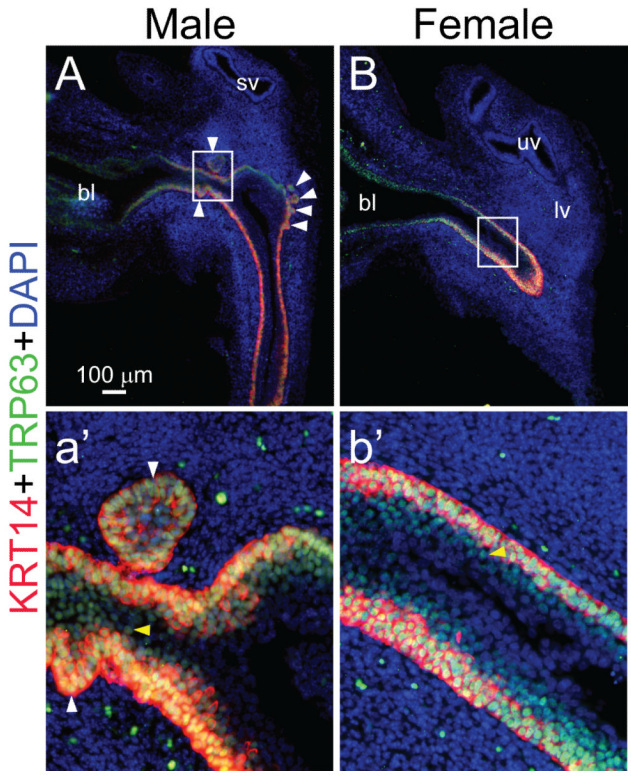

Fig. 2.

KRT14 protein is more selective than TRP63 protein for marking basal urothelial cells in the 17 dpc mouse urethra. (**A, a'**) 17 dpc male and (**B, b'**) female mouse LUT near mid-sagittal sections (5 μm) were stained by immunofluorescence to detect keratin 14 (KRT14, red) and transformation related protein 63 (TRP63, green). Cell nuclei were stained with DAPI (blue). Staining patterns in each panel are representative of three males and three females. Abbreviations used are BL: bladder, ED: ejaculatory duct, LV: lower vagina, SV: seminal vesicle, UV: upper vagina. White arrowheads indicate prostatic buds. Yellow arrowheads indicate $KRT14^{-};TRP63^{+}$ intermediate urothelial cells. All images are of the same magnification.

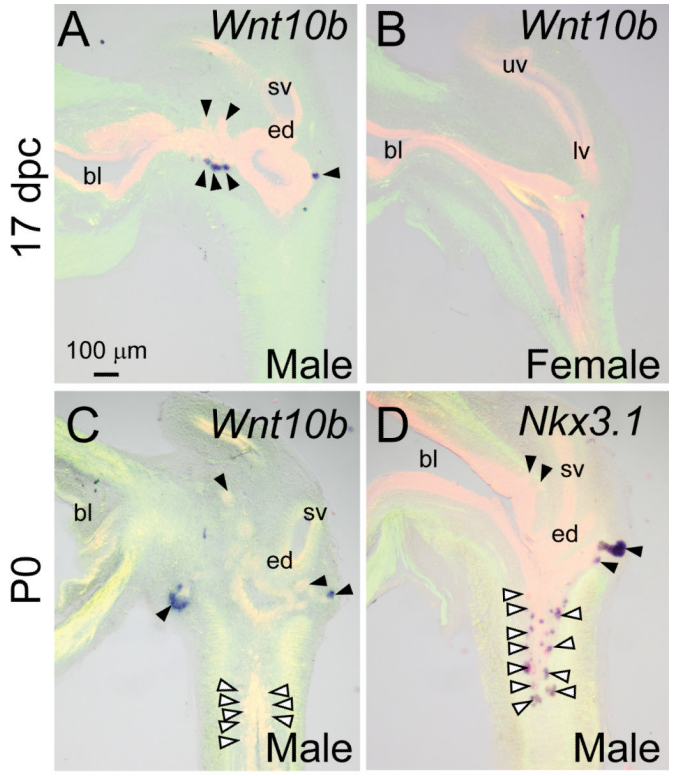

Fig. 3.

Wnt10b is a selective and early stage marker of mouse prostate identity. ISH was used to visualize expression of wingless-related MMTV integration site 10B (*Wnt10b*) mRNA (purple) in near mid-sagittal sections (50 μm) of 17 dpc (**A**) male and (**B**) female mouse LUT. ISH was also used to compare, after formation of prostatic buds and urethral gland buds in P0 male LUT, (**C**) *Wnt10b* and (**D**) NK-3 transcription factor, locus 1 (*Nkx3-1*) mRNA expression. Sections were then stained by immunofluorescence with an anti-smooth muscle actin alpha 2 (ACTA2) antibody that recognizes muscularis mucosa and muscularis propria (green) and an anti-cadherin 1 (CDH1) antibody that recognizes all urothelium (red). Staining patterns are representative of three separate LUTs for each transcript and embryonic stage. Abbreviations used are BL: bladder, ED: ejaculatory duct, LV: lower vagina, SV: seminal vesicle, UV: upper vagina. Black arrowheads indicate representative prostatic buds. White arrowheads indicate representative urethral buds. All images are of the same magnification.

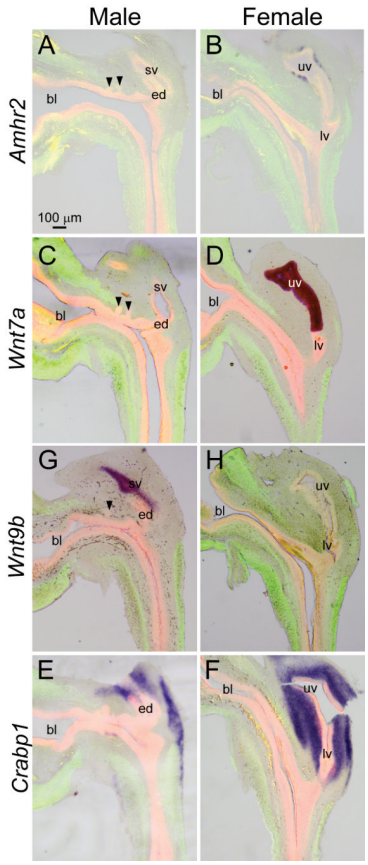

Fig. 4.

Selective mRNA markers of vagina and ejaculatory duct in 17 dpc mice. Near mid-sagittal sections (50 μm) of 17 dpc male and female LUT were stained by ISH to visualize mRNA expression (purple) of (**A-B**) the ejaculatory duct mesenchyme marker anti-Müllerian hormone receptor, type II (*Amhr2*), (**C-D**) the upper vagina epithelium marker wingless-related MMTV integration site 7a (*Wnt7a*), (**E-F**) the seminal vesicle epithelium marker *Wnt9b*, and (**G-H**) the seminal vesicle mesenchyme marker cellular retinoic acid binding protein I (*Crabp1*). Sections were then stained by immunofluorescence with an anti-smooth muscle actin alpha 2 (ACTA2) antibody that recognizes muscularis mucosa and muscularis propria (green) and an anti-cadherin 1 (CDH1) antibody that recognizes all urothelium (red). Staining patterns are representative of three males and three females. Abbreviations used are BL: bladder, ED: ejaculatory duct, LV: lower vagina, SV: seminal vesicle, UV: upper vagina. Arrowheads indicate prostatic buds. All images are of the same magnification.

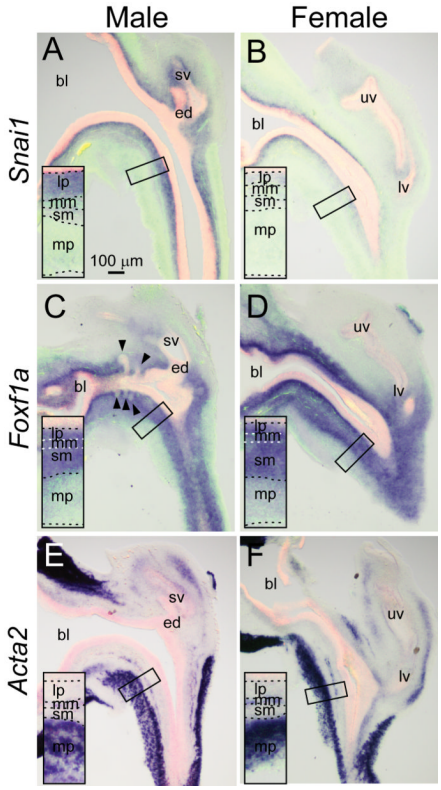

Fig. 5.

Selective mRNA markers of 17 dpc mouse pelvic urethra lamina propria, muscularis mucosa, submucosa, and muscularis propria. Near mid-sagittal sections (50 μm) of 17 dpc male and female LUT were stained by ISH to visualize mRNA expression (purple) of (**A-B**) the lamina propria marker snail homolog 1 (*Snai1*), (**C-D**) the lamina propria and submucosa marker forkhead box f1a (*Foxf1a*), and (**E-F**) the muscularis mucosa and muscularis propria marker actin alpha 2 (*Acta2*). Sections were then stained by immunofluorescence with an anti-smooth muscle actin alpha 2 (ACTA2) antibody that recognizes muscularis mucosa and muscularis propria (green) and an anti-cadherin 1 (CDH1) antibody that recognizes all urothelium (red). Inset images are magnified sections of mesenchyme that reveal the lamina propria (lp), muscularis mucosa (mm), submucosa (sm), and muscularis propria (mp) compartments. Staining patterns are representative of three males and three females. Abbreviations used are BL: bladder, ED: ejaculatory duct, LV: lower vagina, SV: seminal vesicle, UV: upper vagina. All images are of the same magnification.

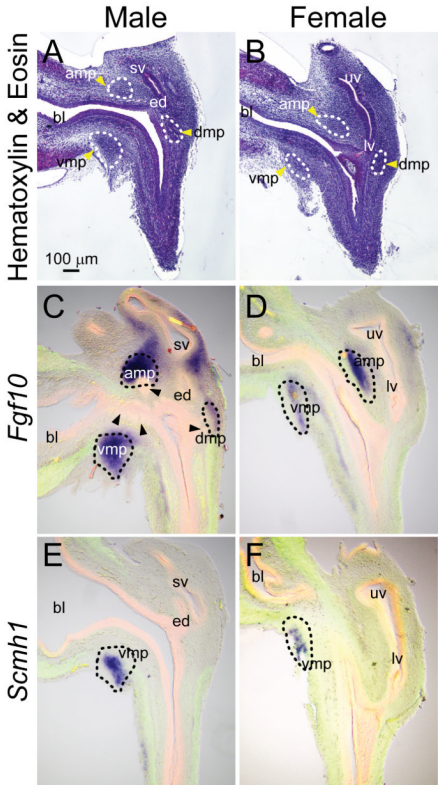

Fig. 6.

Selective mRNA markers of mesenchymal pads of 17 dpc mouse pelvic urethra mesenchyme. (**A-B**) Near mid-sagittal sections (5 μm) of 17 dpc male and female LUT were stained with hematoxylin and eosin to reveal mesenchymal cell condensates that comprise the three mesenchymal pads of the pelvic urethra. Mesenchymal condensates are outlined with dashed lines. (**C-F**) Near mid-sagittal sections (50 μm) of 17 dpc male and female LUT were stained by ISH to visualize mRNA expression (purple) of (**C-D**) fibroblast growth factor 10 (*Fgf10*) that marks all mesenchymal pads and (**E-F**) sex comb on midleg homolog 1 (*Scmh1*) that marks only the ventral mesenchymal pad. Sections were then stained by immunofluorescence with an anti-smooth muscle actin alpha 2 (ACTA2) antibody that recognizes muscularis mucosa and muscularis propria (green) and an anti-cadherin 1 (CDH1) antibody that recognizes all urothelium (red). Results in each panel are representative of three males and three females. Abbreviations used are AMP: anterior mesenchymal pad, BL: bladder, DMP: dorsal mesenchymal pad, ED: ejaculatory duct, LV: lower vagina, MP: muscularis propria, SV: seminal vesicle, UV: upper vagina, VMP: ventral mesenchymal pad. All images are of the same magnification.

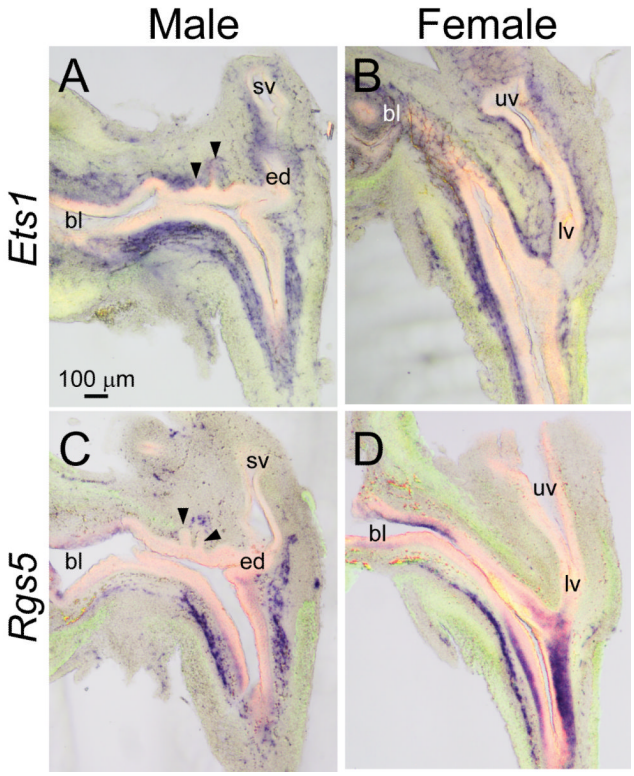

Fig. 7.

Selective mRNA markers of vascular endothelium and pericytes in 17 dpc mouse pelvic urethra. Near mid-sagittal sections (50 μm) of 17 dpc male and female LUT were stained by ISH to visualize mRNA expression (purple) of (**A-B**) the vascular endothelium marker E26 avian leukemia oncogene 1, 5′ domain (*Ets1*) and (**C-D**) the presumptive pericyte marker regulator of G-protein signaling 5 (*Rgs5*). Sections were then stained by immunofluorescence with an anti-smooth muscle actin alpha 2 (ACTA2) antibody that recognizes muscularis mucosa and muscularis propria (green) and an anti-cadherin 1 (CDH1) antibody that recognizes all urothelium (red). Results in each panel are representative of three males and three females. Abbreviations used are BL: bladder, ED: ejaculatory duct, LV: lower vagina, MM: muscularis mucosa, MP: muscularis propria, UV: upper vagina. Arrowheads indicate prostatic buds. All images are of the same magnification.

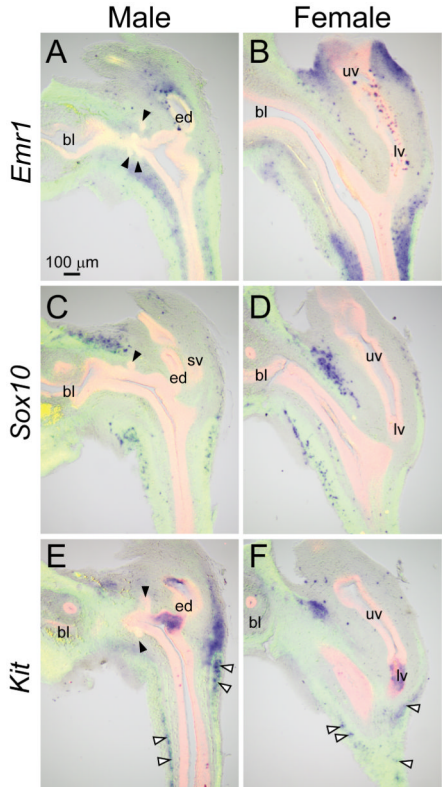

Fig. 8.

Selective mRNA markers of presumptive neural crest cells, macrophages, and interstitial cells of Cajal in 17 dpc mouse pelvic urethra. Near mid-sagittal sections (50 μm) of 17 dpc male and female LUT were stained by ISH to visualize mRNA expression (purple) of (**A-B**) the presumptive macrophage marker egf-like module containing, mucin-like, hormone receptor-like 1 (*Emr1*), (**C-D**) the presumptive neural crest derived cell marker SRY (sex determining region Y)-box 10 (*Sox10*), and (**E-F**) the presumptive interstitial cell of Cajal (ICC) marker kit oncogene (*Kit*). Sections were then stained by immunofluorescence with an anti-smooth muscle actin alpha 2 (ACTA2) antibody that recognizes muscularis mucosa and muscularis propria (green) and an anti-cadherin 1 (CDH1) antibody that recognizes all urothelium (red). Results in each panel are representative of three males and three females. Abbreviations used are BL: bladder, ED: ejaculatory duct, LV: lower vagina, MM: muscularis mucosa, MP: muscularis propria, UV: upper vagina. Black arrowheads indicate prostatic buds and white arrowheads indicate presumptive ICC. All images are of the same magnification.

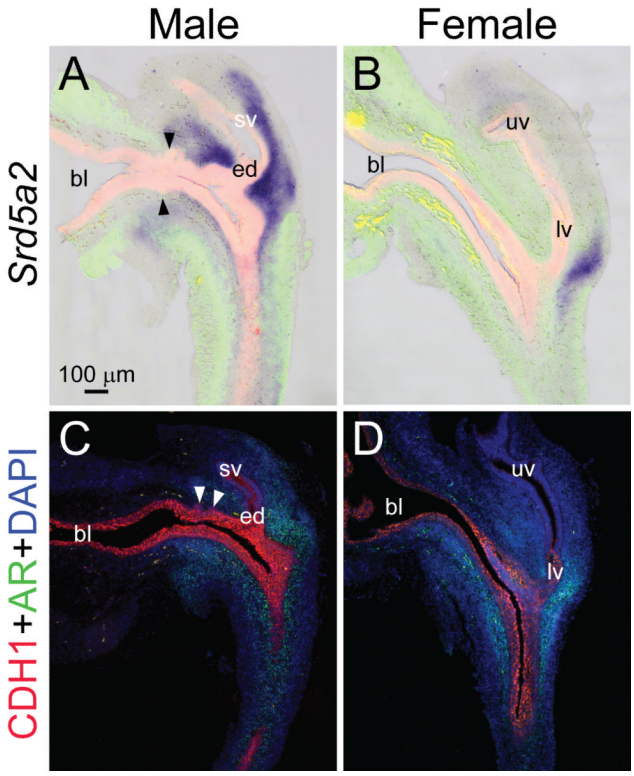

Fig. 9.

Srd5a2 mRNA expression marks a sub-population of 17 dpc male LUT stroma where nuclear androgen receptor protein expression is abundant. Near mid-sagittal sections (50 μm) of 17 dpc male and female LUT were stained by ISH to visualize mRNA expression (purple) of (**A-B**) steroid 5 alpha reductase type 2 (*Srd5a2*). Sections were then stained by immunofluorescence with an anti-smooth muscle actin alpha 2 (ACTA2) antibody that recognizes muscularis mucosa and muscularis propria (green) and an anti-cadherin 1 (CDH1) antibody that recognizes all urothelium (red). In panels **C-D**, IHC was used to visualize the distribution of nuclear androgen receptor (AR) protein (green). CDH1 (red) was used to visualize urothelium and DAPI (blue) was used to visualize cell nuclei. Results in each panel are representative of three males and three females. Abbreviations used are BL: bladder, ED: ejaculatory duct, LV: lower vagina, MM: muscularis mucosa, MP: muscularis propria, UV: upper vagina. Arrowheads indicate prostatic buds. All images are of the same magnification.

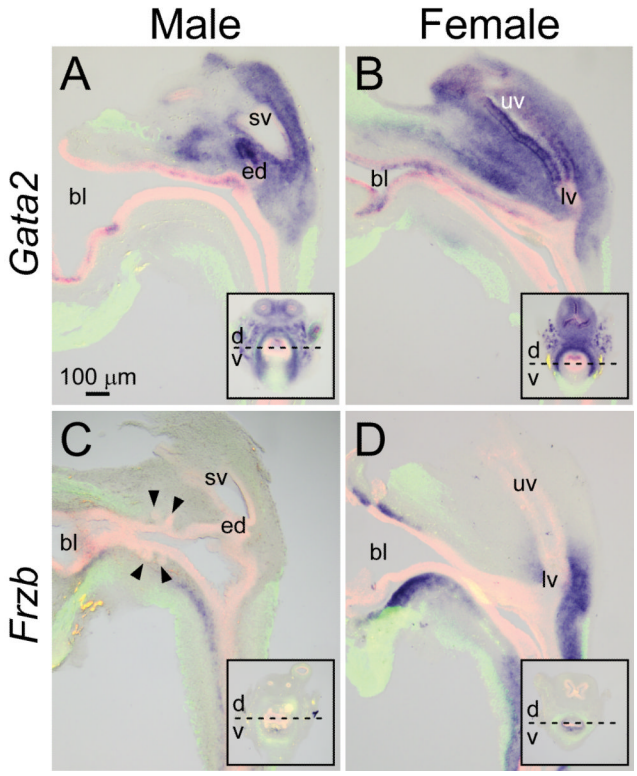

Fig. 10.

Selective mRNA marker of dorsal LUT in 17 dpc mice. Near mid-sagittal sections (50 μm) of 17 dpc male and female LUT were stained by ISH to visualize mRNA expression (purple) of (**A**-**B**) the dorsal urethral marker GATA binding protein 2 (*Gata2*) and (**C**-**D**) the ventral urethral marker frizzled-related protein (*Frzb*). Sections were then stained by immunofluorescence with an anti-smooth muscle actin alpha 2 (ACTA2) antibody that recognizes muscularis mucosa and muscularis propria (green) and an anti-cadherin 1 (CDH1) antibody that recognizes all urothelium (red). Inset images are transverse sections (50 μm) of 17 dpc male and female LUT. Results in each panel are representative of three males and three females. Abbreviations used are BL: bladder, D: dorsal, ED: ejaculatory duct, LV: lower vagina, UV: upper vagina, V: ventral. Arrowheads indicate prostatic buds. All images are of the same magnification.

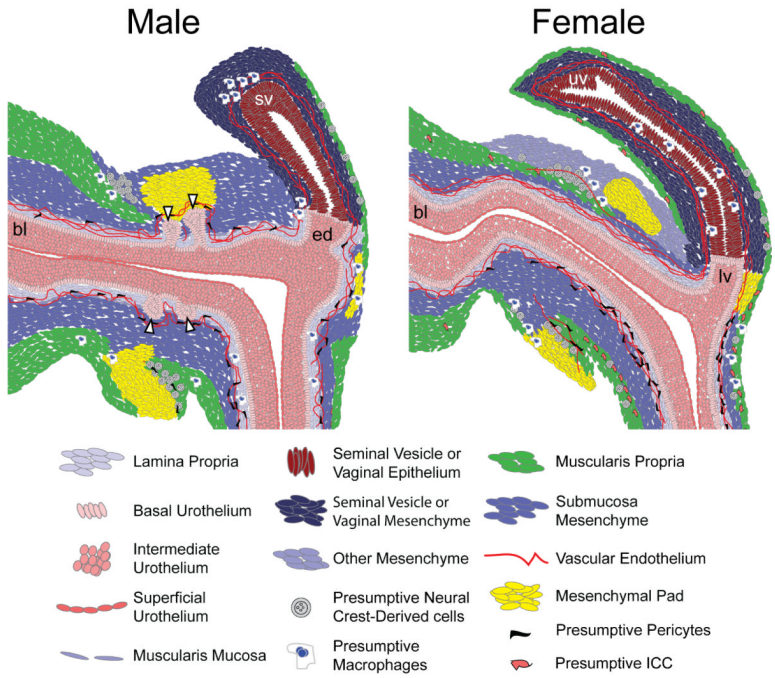

Fig. 11.

Schematic representation of stromal and epithelial sub-compartments in 17 dpc mouse LUT. A representation of a near mid-sagittal 17 dpc mouse LUT is shown and tissue sub-compartments identified in the current study are color-coded according to the key. Supplemental Fig. 1. Functional androgen receptor signaling is required for *Srd5a2* mRNA expression in the mouse UGS. (**A**) E14.5 male C57BL/6J fetal mouse UGS tissues were incubated for 24 hr in organ culture media containing 10 μm hydoxyflutamide (OHF, androgen receptor [AR] antagonist) or 10 nM 5α dihydrotestosterone (DHT, AR agonist). (**B)** UGS tissues were collected from male E18.5 wild type fetal mice that harbor a functional *Ar* and from testicular feminization (*Tfm*) fetal mice that harbor a spontaneous *Ar* mutation that renders it less sensitive to androgens. *Srd5a2* mRNA abundance was assessed by real-time RT-PCR and normalized to peptidyl prolyl isomerase mRNA abundance. Results are mean ± SE of n = 3 litter-independent samples per group. Significant differences from the control group ($p < 0.05$) are indicated by an asterisk and were identified by Student's T-Test.